Composites Part B 91 (2016) 422–430

Contents lists available at ScienceDirect

Composites Part B

journal homepage: www.elsevier.com/locate/compositesb

Development of high-performance resin nanocomposites by resin cellulation using multi-walled carbon nanotubes

Shigeki Inukai [a, *], Toru Noguchi [a, e], Ken-ichi Niihara [b], Morio Aoki [b], Masaharu Miura [c], Eisuke Yamada [d], Kenji Takeuchi [a, e], Morinobu Endo [a, e]

[a] Global Aqua Innovation Center, Shinshu University, 4-17-1 Wakasato, Nagano 380-8553, Japan
[b] Nissin Kogyo Co. Ltd., 801 Kazawa, Tomi, Nagano 386-8505, Japan
[c] Iida Industry Co. Ltd., 1-5 Numa Kitaohmi, Inazawa, Aichi 492-8547, Japan
[d] Department of Applied Chemistry, Aichi Institute of Technology, 1247 Yachigusa Yakusa, Toyota, Aichi 470-0392, Japan
[e] Institute of Carbon Science and Technology, Shinshu University, 4-17-1 Wakasato, Nagano-shi 380-8553, Japan

ARTICLE INFO

Article history:
Received 8 May 2015
Received in revised form
17 December 2015
Accepted 26 December 2015
Available online 3 February 2016

Keywords:
A. Polymer-matrix composites (PMCs)
A. Thermoplastic resin
B. High-temperature properties
B. Mechanical properties

ABSTRACT

This work aims to enhance resin reinforcing performance and thermal resistance through the innovative use of multi-walled carbon nanotubes (MWCNTs) for advanced material applications. The new method, which relied on MWCNT disentanglement under high shear stress, produced resin matrix nanocomposites. The MWCNT/resin nanocomposites showed improved stiffness without significant flexibility loss and did not flow above 160 °C. These dramatic improvements may result from the formation of a three-dimensional structure at the MWCNT/resin interface.

1. Introduction

Carbon nanotubes (CNTs) were synthesized by catalytic vapour growth for the first time in 1976 [1,2] but were only analysed in 1991 [3]. In addition to numerous synthetic processes exploiting various vacuum technologies, their unique properties have attracted considerable attention for the development of advanced materials.

Initial polymer-based composite materials using CNTs as fillers involved epoxy resin [4–18], polypropylene [19–34], polycarbonate [35–38] and polyamide [39–42]. These CNT fillers have remarkably enhanced polymer electrical properties [4,5,14,25–28], thermal conductivity [6,29,42,43], and crystallinity [30–32,39,40]. They have also boosted resin mechanical characteristics [4,7–18,21,22,27–34,36–38,40–42]. However, these mechanical improvements have been predominantly restricted to CNT filling rates lower than 10 vol% and, thus, remain limited compared to electrical and thermal conductivity enhancements. The rarity of high-filled CNT/polymer composites stems from existing challenges in generating uniform dispersions at high CNT concentrations. Despite the existence of low-filled composites featuring improved mechanical properties, few studies have achieved CNT dispersions at the macro-nanoscale [30,32,37,41,42] instead of the nanoscale. In addition, the composites exhibited rather poor flexibility, even at filling concentrations of wt% [4,9,17,33,40], which indicates that uniform CNT dispersions remain problematic.

Attempts at generating uniform dispersions include CNT surface chemical treatment [10,11,16,19,34], masterbatch application [22,29] and mechanical treatment by biaxial milling using high shear force [8,11,18,20,21]. However, chemical treatments encounter problems regarding their industrial applicability, such as post-processing liquid-waste disposal under strict conditions. Biaxial milling using a high shear force produces CNT clumps at the microscale. Therefore, neither of these methods provides uniform dispersions at the nanoscale, suggesting their inability to facilitate the exploitation of CNTs as nanofillers.

An elasto-milling method utilizing the polarity and free radical effect in addition to the elastomer-specific viscosity and elasticity has been developed to process rubber and elastomer materials. This method produced a composite in which multiwalled carbon nanotubes (MWCNTs) were disentangled in an elastomer matrix, resulting in excellent thermal and mechanical properties [44–46].

* Corresponding author.
E-mail address: inukai@endomoribu.shinshu-u.ac.jp (S. Inukai).

http://dx.doi.org/10.1016/j.compositesb.2015.12.039
1359-8368/

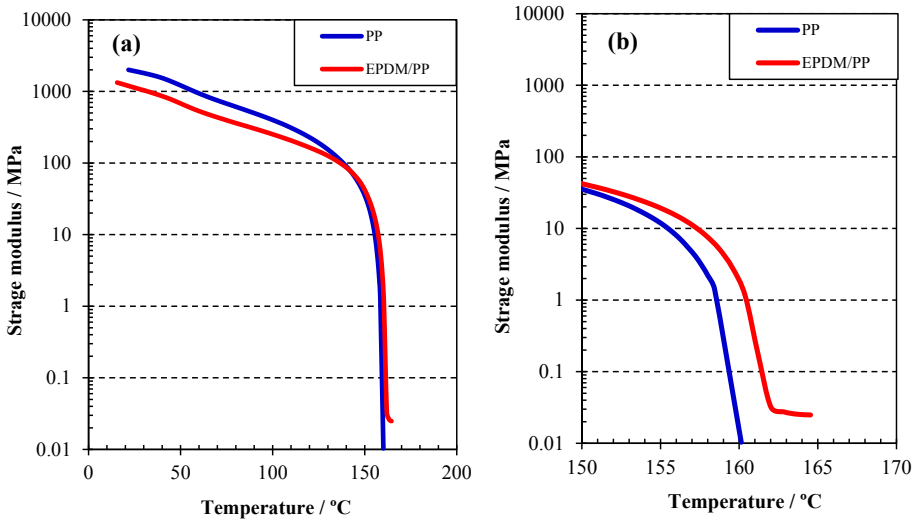

Fig. 1. Storage elastic moduli of PP and EPDM/PP as a function of temperature. (a) Full temperature range and (b) 150–170 °C range.

This disentanglement relies on a cellulation mechanism, in which MWCNTs and matrix robustly form a three-dimensional nano-continuous structure [45–47]. This cellulation technology has generated several composites and has found application in an increasing number of areas [48–50].

The elasto-milling process was developed to enhance elasticity and shear force at low temperature, resulting in extremely high-performance rubber reinforced with MWCNTs [48]. An effective process hinges on several matrix-related requirements. (1) Elastomer molecules forming the matrix need to fill the voids created by the physically intermingled nanotubes, effectively breaking their inherent agglomeration during mixing. (2) The matrix has to exhibit good 'wettability' with carbon nanotubes and (3) its elasticity facilitates kneading. However, many resins do not meet this third processing condition because of their lack of elasticity.

Because of its dependence on elastomer-specific elasticity, the elasto-milling method has proven difficult to apply to resins. Nonetheless, this problem was addressed by blending a resin with an elastomer to reveal an elastic region. In addition, a elasto-milling method that facilitates MWCNT disentanglement in a resin matrix was developed. Along with a description of this resin-specific method, the physical properties of the obtained MWCNT/resin composites and resin cellulation were evaluated.

2. Experimental

2.1. Materials

Polypropylene (PP, Admer QE800) and ethylene propylene rubber (EPDM, Tafmer MH7020) were purchased from Mitsui

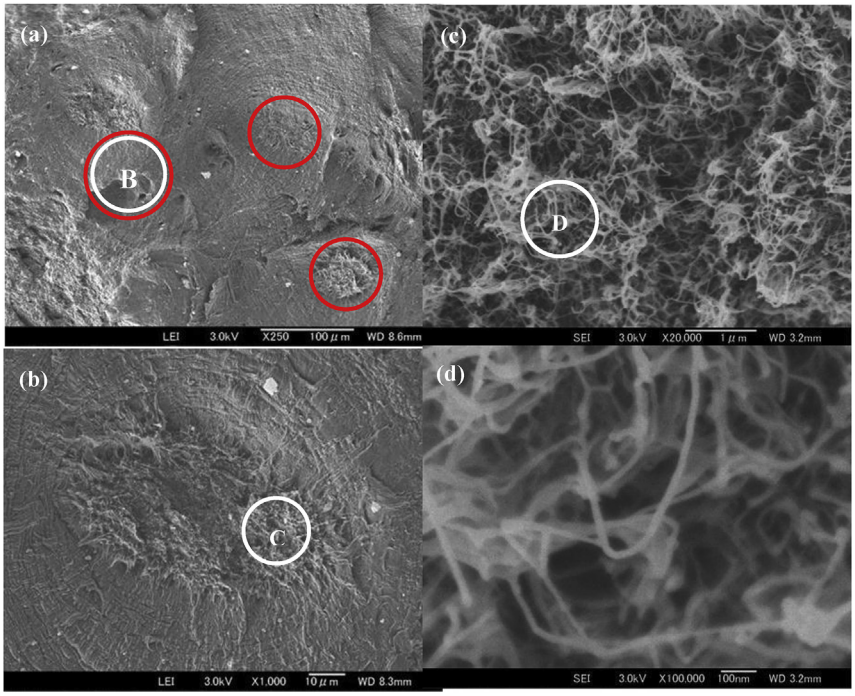

Fig. 2. Cross-sectional SEM images of 10 wt% Ref: (a) Full image, (b) magnification of part B, (c) magnification of part C, and (d) magnification of part D.

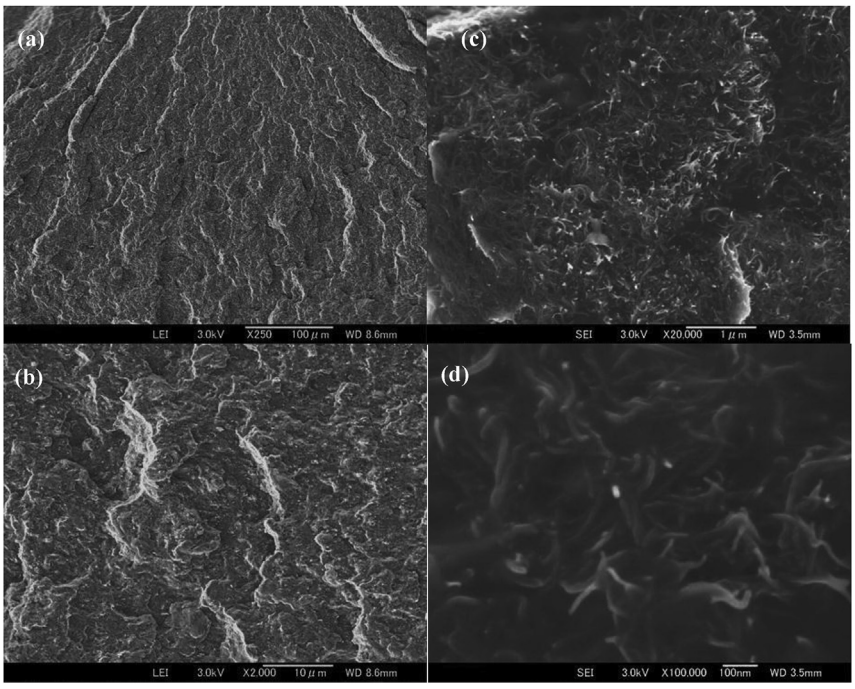

Fig. 3. Cross-sectional SEM images of 10 wt% Comp: (a) ×250, (b) ×2,000, (c) ×20,000 and (d) ×100,000.

Chemicals, Inc. MWCNTs (NC-7000, average diameter: 10 nm) were acquired from Nanocyl.

2.2. Nanocomposite preparation

Polypropylene (200 g) and EPDM (50 g) were placed in a closed kneading machine (Brabender) at 200 °C and a mixing rate of 200 rpm. Next, a predetermined quantity of nanocarbon was added for further mixing to obtain a concentration of 5, 10, 15 or 20 wt% in the EPDM/PP matrix. The mixture was cut to a predetermined length using a pelletizer to form a pellet. This sample made by ordinary viscosity milling was used as a reference. The produced pellet was processed in a 3-inch open two-roll mill heated to 162–165 °C and allowed to wrap itself around the rolls. The composite was tight-milled for 5 min with a nip gap of 0.1 mm to achieve an extremely high shear force and subsequently cut into a new pellet using a pelletizer. This pellet was filled into a 150 × 180 mm × 1 mm metal mould and was hot pressed at 200 °C for 5 min in a vacuum moulding machine to produce a specimen. Hereafter, samples formed by viscosity milling will be called x wt% Ref and their fully processed analogues will be called x wt% Comp.

2.3. Characterization and mechanical testing

Freeze-fracture cross-sections were examined by field-emission scanning electron microscopy (FE-SEM) using a JSM7400-F instrument (JEOL Ltd). Transmission electron microscopy (TEM) images were acquired on a JES-2200FS apparatus (JEOL Ltd) operating at an acceleration voltage of 200 kV. Ultrathin composite sections presenting thicknesses of approximately 100 nm were cut using a Leica Ultracut UCT ultra microtome equipped with a diamond knife.

Tensile property measurements were performed at 23 °C and a tensile speed of 50 mm/min according to ISO 527-1. The produced pellet was moulded into a No.1 dumbbell-type piece using an injection moulding machine LA-150 (Sodick Plustech Co., Ltd).

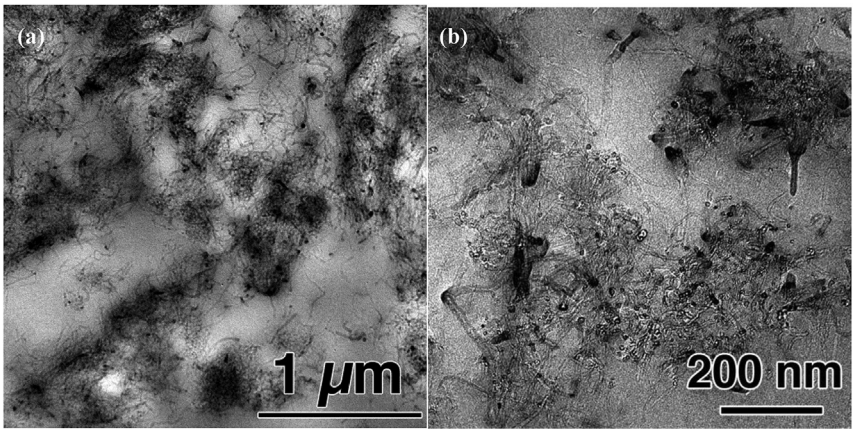

Fig. 4. Cross-sectional TEM images of 10 wt% Comp: (a) ×5000 and (b) ×20,000.

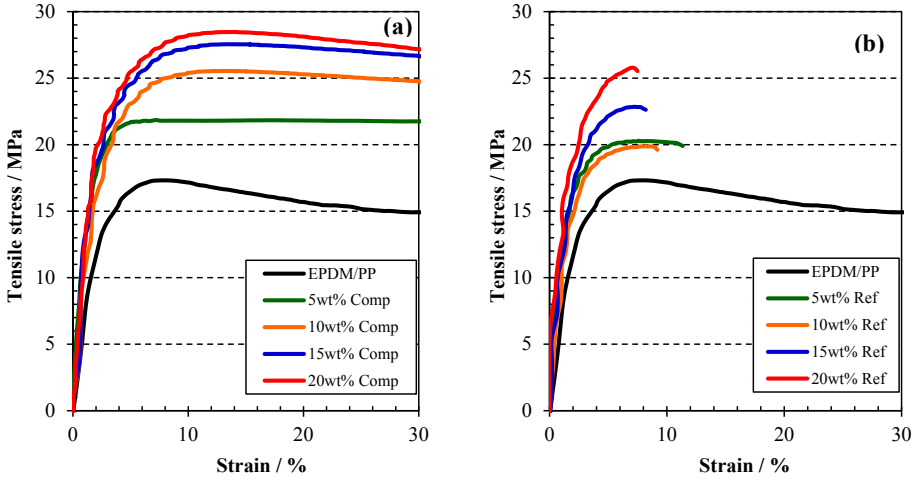

Fig. 5. Stress–strain curves of MWCNT/EPDM/PP composites: (a) 5, 10, 15 and 20 wt% Comp and (b) 5, 10, 15 and 20 wt% Ref. Strain magnification: 0%–30%).

Table 1
Tensile properties of 5, 10, 15 and 20 wt% Comp and 5, 10, 15 and 20 wt% Ref.

Item	Comp			Ref		
Content [wt%]	Y_S [MPa][a]	T_S [MPa][b]	E_B [%][c]	Y_S [MPa][a]	T_S [MPa][b]	E_B [%][c]
0	17.3	14.6	400	17.3	14.6	400
5	21.8	18.6	145	Rupture	19.9	11
10	25.5	21.0	85	Rupture	19.6	9
15	27.6	24.5	55	Rupture	22.6	8
20	28.5	26.0	40	Rupture	25.5	7

[a] Y_S [MPa]: Yield stress.
[b] T_S [MPa]: Tensile stress at break
[c] E_B [%]: Elongation at break.

Dynamic mechanical analysis (DMA) was performed under the tensile mode using a dynamic viscoelasticity measuring device (DMS6100; SII) under certain conditions. The specimen measured 1.0 mm × 4.0 mm × 40 mm, the distance between chucks was 20 mm, the temperature ranged between 20 and 300 °C and increased at 1.5 °C/min, and the frequency equalled 1 Hz.

Linear expansion coefficients were measured using a thermomechanical analysis device (TMA6100; SII) for a 1.0 mm × 2.0 mm × 20 mm specimen and a distance of 10 mm between chucks. Dimensional variations were evaluated between −100 and 300 °C in air for a length measurement load of 25 kPa and a heating rate of 3 °C/min. The differential value of the linear expansion coefficient was calculated every 1 °C.

A master curve of the relaxation modulus was obtained through a tensile stress relaxation test using a thermomechanical analysis device (TMA6100; SII) at room temperature. The specimen measured 1.0 mm × 2.0 mm × 20 mm, the distance between chucks equalled 10 mm, and the distortion amounted to 1%. The obtained master curve was processed using finite element method software (MSC Marc®, MSC Software) and viscoelastic constants were calculated.

3. Results and discussion

3.1. Resin elasto-milling method

First, we will explain the resin elasto-milling method developed in this research. Fig. 1 shows the temperature dependence of the storage elastic moduli of PP (E'_{PP}) and an EPDM/PP composite containing 20 wt% EPDM ($E'_{EPDM/PP}$). When the temperature increases, the modulus E'_{PP} decreases gradually upon polymer softening and then sharply above 120 °C before becoming immeasurable above approximately 160 °C at the polymer elongation limit (Fig. 1(a)). The modulus $E'_{EPDM/PP}$ exhibits a quasi-similar behaviour except at high temperature (Fig. 1(b)). Despite a narrow stable region is observed between 162 and 165 °C, $E'_{EPDM/PP}$ becomes immeasurable at higher temperatures because the elongation limit of the composite is reached. If EPDM/PP is kneaded in this narrow temperature region, its elasticity makes mixing

Table 2
Elastic moduli, relaxation times, and viscosity coefficients of EPDM/PP, 10 wt% Ref, and 10 wt% Comp obtained by model fitting.

		Unit	Neat	Comp	Ref
Mixing		wt%	Viscosity milling	Elasto-milling	Viscosity milling
Content			0	10	10
Strain amount		%	1.0	1.0	1.0
Elastic modulus	E_e	N/mm^2	96	141	45
	E_1	N/mm^2	7	8	3
	E_2	N/mm^2	5	132	5
	E_3	N/mm^2	26	20	22
Relaxation time	τ_1	sec	475	1500	375
	τ_2	sec	650	220	1200
	τ_3	sec	3550	5500	3550
Viscosity coefficient	η_1	N_{sec}/mm^2	3189	11,849	1089
	η_2	N_{sec}/mm^2	3108	28,935	5461
	η_3	N_{sec}/mm^2	91,404	108,616	79,052

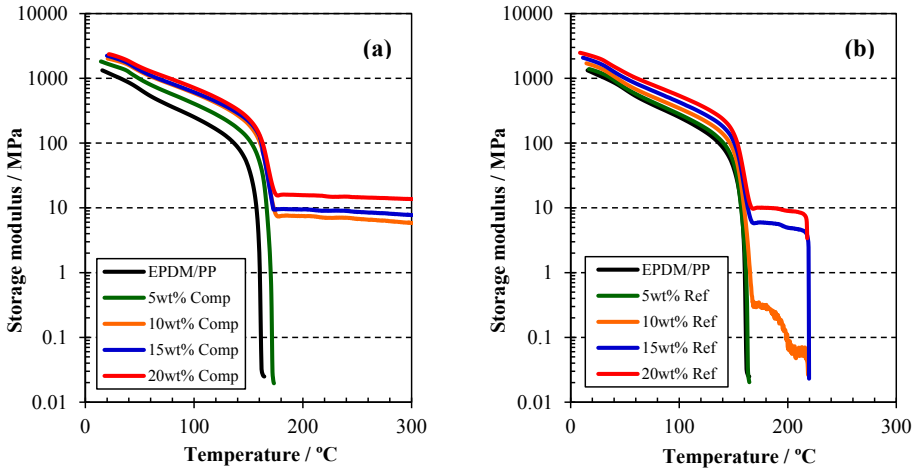

Fig. 6. Storage moduli of MWCNT/EPDM/PP composites as a function of temperature: (a) 5, 10, 15 and 20 wt% Comp and (b) 5, 10, 15 and 20 wt% Ref.

possible. High shear stress exerted during mixing may induce MWCNT disentanglement. Specifically, molecules get highly distorted by the large shear force when they pass through the roll. However, rubber's recovery force restores its original structure immediately after passing through the roll. These repeated distortion and recovery steps during plastic kneading may extract CNTs from the cohesive group thread by thread, resulting in their disentanglement [46,48]. The resin elasto-milling method depends on this 162–165 °C region, which emerges for an added EPDM amount of 5 wt%.

3.2. Composite morphologies

Fig. 2 shows freeze-fracture cross-sectional SEM images of 10 wt % Ref produced by ordinary viscosity milling. MWCNT clumps are observed at low magnification (Fig. 2(a), red circle). These clumps

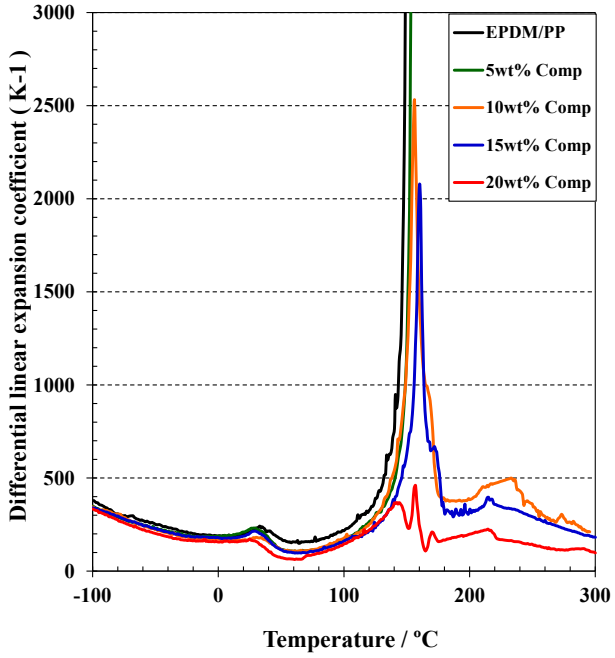

Fig. 7. Differential linear expansion coefficients (K-1) of Comp specimens determined by TMA.

approximate 100 μm (Fig. 2(b)) and are located near the raw material (Fig. 2(c) and (d)). Therefore, MWCNT clumps measuring several tens to a hundred microns in diameter are present in specimens produced by ordinary viscosity milling and form a sea island structure. In other words, ordinary viscosity milling cannot disentangle MWCNTs in an EPDM/PP matrix. Fig. 3 shows freeze-fracture cross-sectional SEM images of 10 wt% Comp produced by resin elasto-milling. No MWCNT clumps are observed at low magnification (Fig. 3(a)). The edge of the MWCNT appears as a bright, white dot at higher magnification (Fig. 3(b)). Moreover, no sea island structure, characteristic of poor dispersion, is detected, suggesting that MWCNTs are disentangled in the matrix. Furthermore, the MWCNT root portion and interface with the matrix show no crack while no hole is present in the matrix (Fig. 3(c)), indicative of good MWCNT/matrix adhesion. Fig. 4 shows TEM images of an ultrathin composite specimen with the same additive amount (10 wt% Comp) generated by resin elasto-milling. The polymer matrix permeates the MWCNTs, separating them individually.

When MWCNTs are first mixed with the matrix at 200 °C in the closed kneading machine to prepare the composites, EPDM/PP molecules infiltrate the raw material clumps because of their viscous flow. Good wettability is obtained between MWCNTs and EPDM/PP as a result of van der Waals interactions. In addition, the heated open two-roll mill generates a strong shear force by elastic kneading, considerably transforming the mixture. However, once the shear force is removed, a resilient force is created, immediately restoring the original mixture. Repeating these transformation and restoration steps pulled individual MWCNTs out of the clumps, disentangling them one by one.

3.3. Nanocomposite mechanical and thermal properties

Fig. 5 (a) and (b) show stress–strain (S–S) curves of the 0–100% distortion regions of Comp and Ref, respectively. Table 1 lists the values for yield stress (Y_S), tensile strength (T_S), and elongation at break (E_B) obtained from the tensile testing of Comp and Ref. Neat EPDM/PP presents a yield point at approximately 15% distortion and subsequent necking before finally breaking at 400% distortion. The S–S curve of Comp displays an increase in yield stress with increasing MWCNT content (Fig. 5(a)). This results from the extremely high aspect ratio, disentanglement, good EPDM/PP matrix adhesiveness of the MWCNTs. Tensile strength and elongation at break tend to decrease with increasing MWCNT filling. However, no breaking is

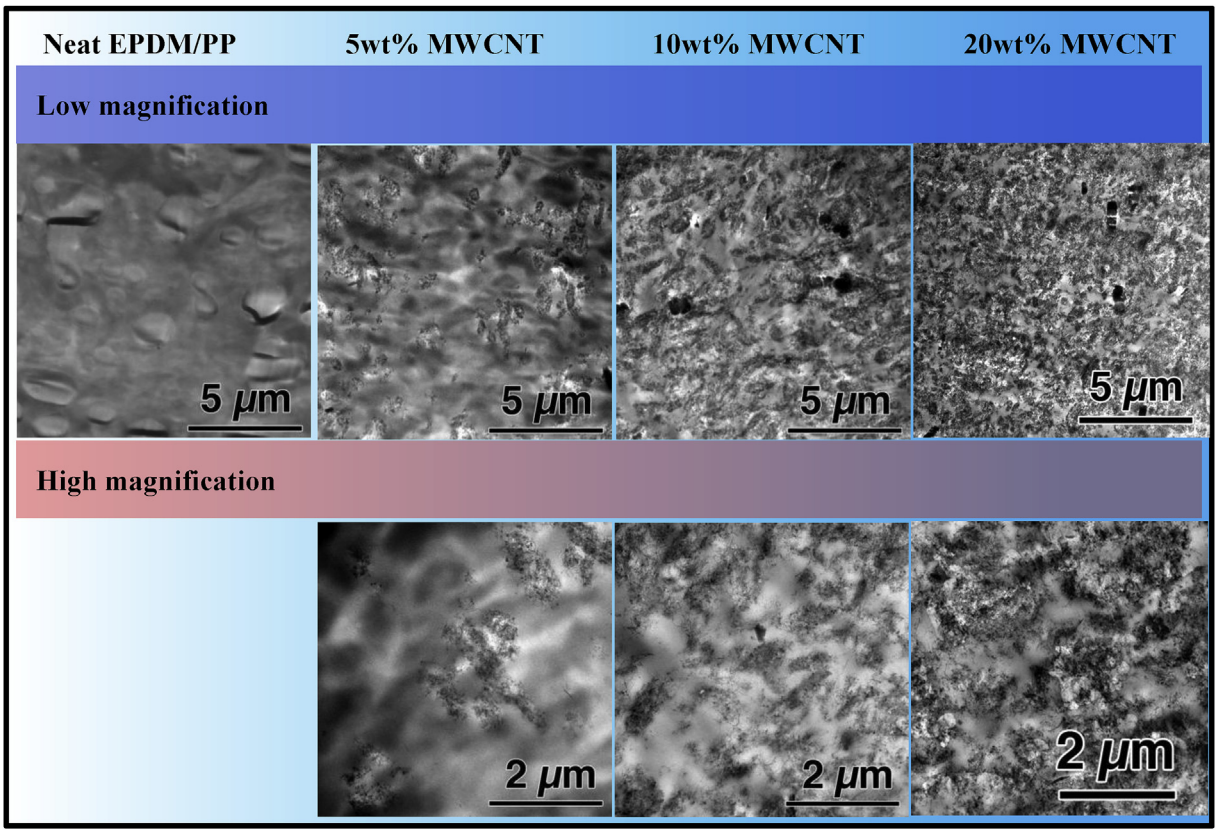

Fig. 8. Cross-sectional TEM images of unstained neat EPDM/PP, 5, 10 and 20 Comp.

observed below several percent of distortion because of the disentangled MWCNTs. In contrast, the S–S curve of Ref shows a complete brittle fracture below the yield point (Fig. 5(b)), consistent with the presence of MWCNT clumps measuring several tens to hundreds of microns in diameters in this composite (Fig. 2). Applied stress on the composite creates stress concentration on these hollow clumps, significantly reducing composite tensile properties (Table 1).

The temperature dependence of the storage elastic moduli of fully processed (E'_{Comp}) and reference specimens (E'_{Ref}) are shown in Fig. 6(a) and (b), respectively. When the temperature increases, the modulus $E'_{EPDM/PP}$ decreases gradually upon polymer softening and then sharply above 120 °C. Despite a narrow stable region is observed between 162 and 165 °C, $E'_{EPDM/PP}$ becomes immeasurable at higher temperatures because the elongation limit of the composite is reached. The modulus E'_{Comp} (Fig. 6(a)) shows a comparable trend to EPDM/PP and increases substantially with increasing MWCNT filling at high temperature. Similarly to neat EPDM/PP, flow occurs in 5 wt% Comp, albeit at higher temperature. However, MWCNT filling slightly suppresses flow. In addition, the stable E′ region emerges between 160 °C, corresponding to neat EPDM/PP flow onset, and 300 °C in specimens with filling amounts exceeding 10 wt%. In contrast, the modulus $E'_{Ref\ rises}$ with increasing MWCNT filling at high temperature (Fig. 6(b)) but this growth remains smaller than for E'_{Comp}. Moreover, the 5 wt% Ref composite reaches in elongation limit at approximately the same temperature as for neat EPDM/PP, indicating that a small amount of entangled MWCNTs displays no reinforcing effect. The modulus E'_{Ref} presents a stable region above 160 °C but remains lower than E'_{Comp}. The 10, 15, and 20 wt% Ref composites become immeasurable at approximately 220 °C because of breakage. This breakage may originate from the existence of numerous MWCNT clumps in the specimens, as suggested during tensile tests.

Fig. 7 shows the differential linear expansion coefficient (K-1) of 5, 10, 15 and 20 wt% Comp as a function of temperature. For neat EPDM/PP and 5 wt% Comp, K-1 greatly increases at about 110 °C because of flow before becoming immeasurable at 120 °C when the elongation limit is reached. In contrast, in 10, 15 and 20 wt% Comp specimens, which show a flat E'_{Comp} region at higher temperature than the DMA melting point, the flow-derived peaks become smaller as the added amount of MWCNTs increases. Finally, almost disappearance of the peak for 20wt% Comp indicates that the incorporated tubes effectively prevent the flow of Neat EPDM/PP.

3.4. Resin cellulation and reinforcement mechanisms

MWCNT/EPDM/PP composites exhibit unique properties, such as the remarkable migration suppression and the emergence of a stable elastic modulus region between the polymer flow onset temperature (160 °C) and 300 °C. Flow suppression and disappearance are detected in composites in which MWCNTs generate a three-dimensional continuous structure at their interface with an elastomer matrix [45–48]. This suggests that a similar cell structure forms in the EPDM/PP matrix. Therefore, evidence for this cell structure was evaluated by TEM and the reinforcement mechanism was analysed by viscosity elasticity modelling.

3.4.1. Composite structure analysis by TEM

Fig. 8 shows low- and high-magnification TEM images of 5, 10, 15 and 20 wt% Comp. The MWCNTs are disentangled in the EPDM/PP in all specimens. The TEM image of 5 wt% Comp displays dense

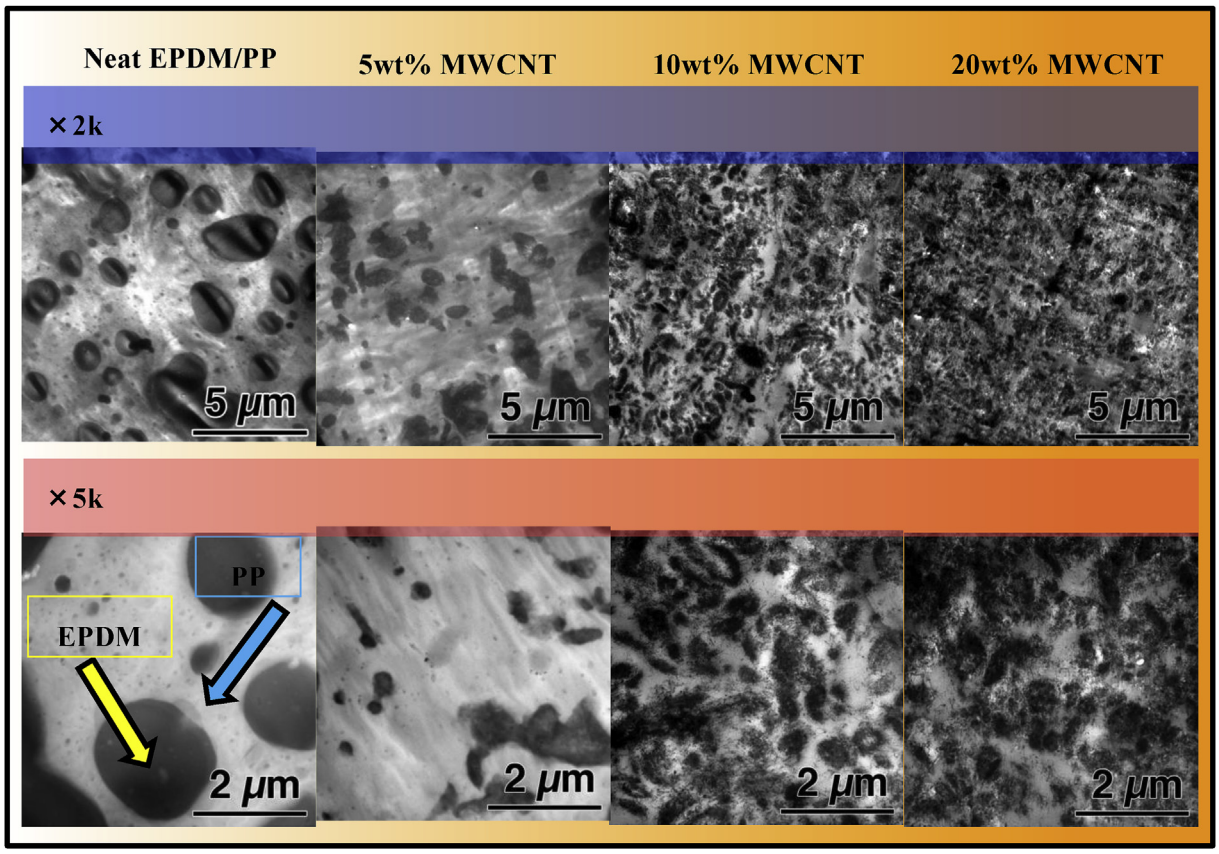

Fig. 9. Cross-sectional TEM images of RuO_4-dyed neat EPDM/PP, 5, 10 and 20 wt% Comp.

and sparse MWCNT portions. The sparse portion shrinks when the filling amount rises from 10 to 15 wt% and disappears at 20 wt% Comp.

Next, a detailed cell formation mechanism was determined by examining phase structures of acid-dyed ultra-thin specimens and neat EPDM/PP by TEM. Fig. 9 shows TEM images of neat EPDM/PP and ruthenium tetroxide (RuO4)-dyed 5, 10, and 20 wt% Comp specimens. Neat EPDM/PP presents black patterns measuring up to ca. 2 μm by TEM. These black patterns correspond to EDPM components blended into PP. Interestingly, the 2 μm-sized EPDM phase exhibits a sea island-type phase separated structure in the PP phase for EPDM/PP. The TEM image of 5 wt% Comp demonstrates that MWCNTs fill the RuO_4-dyed EPDM phase to a greater extent than the non-dyed PP phase. The TEM image of 10 wt% Comp reveals that a cell structure begins to emerge from the RuO_4-dyed EPDM phase. When the filling amount reaches 20 wt%, this structure is present in the entire system, resulting in a three-dimensional continuous arrangement. A cell structure formation

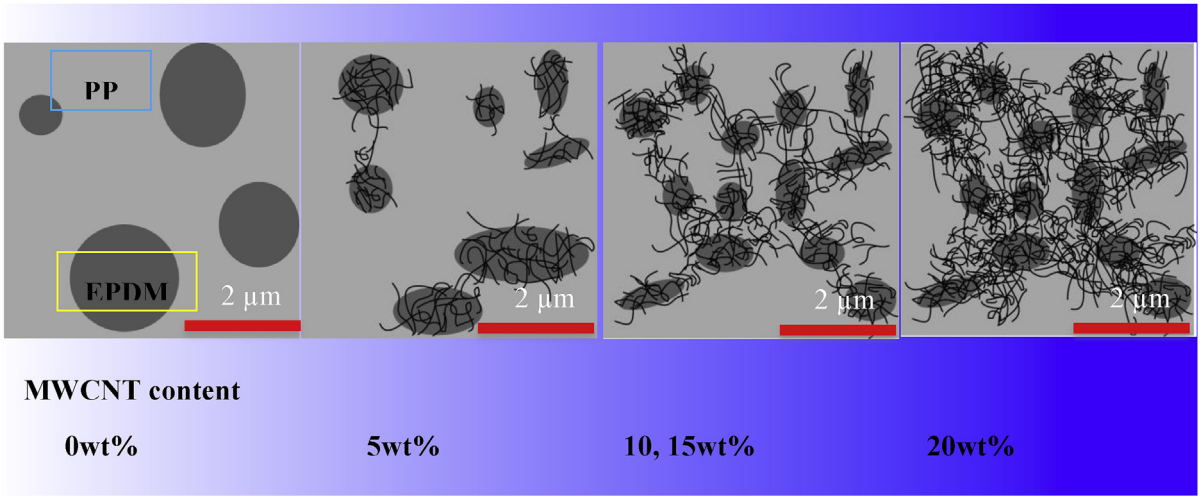

Fig. 10. Proposed cellulation model in MWCNTs/EPDM/PP composites.

mechanism based on this TEM analysis is proposed in Fig. 10. PP and EPDM are phase-separated similarly to a sea island structure. When the MWCNT content reaches 5 wt%, the disentangled MWCNTs (cell aggregates) are greatly dispersed in the EPDM phase, which partly starts to link across the MWCNTs. At 10 wt% MWCNT content, MWCNTs exist in EPDM and PP phases and facilitate the creation of a continuous rubber phase. The occurrence of the stable elastic modulus region and the suppression of migration are observed above 160 °C. When the MWCNT content surpasses 20 wt%, almost all rubber phases are joined through MWCNTs and the flow appears to stop.

3.4.2. Viscoelastic analysis of composites

Resin cellulation composites exhibit distinct properties from their conventional counterparts, which indicates their difference from traditional reinforcement models. Therefore, their structure–property correlation was elucidated by physical modelling. Measurements were performed for neat EPDM/PP, 10 wt% Ref, and 10 wt% Comp.

When the viscoelasticity is analysed using a general-purpose finite element method software, such as MSC Marc®, the elastic modulus must be given as a relaxation elastic modulus G(t) as a function of time t. At constant temperature, a viscoelasticity constitutive equation that relates the stress σ and the distortion ε is expressed as [51]:

$$\sigma(t) = \int_{-\infty}^{t} G(t-\tau)\frac{d\varepsilon(\tau)}{d\tau}\,d\tau \tag{1}$$

The viscoelasticity modelling analysis by a finite element method uses a generalized Maxwell model. Each Maxwell model with a serial connection of springs and dashpots is connected in parallel in k rows [52]. The equation related to the stress-distortion in a generalized Maxwell model is written as [51]:

$$\frac{d\varepsilon_k}{dt} = \frac{1}{G_k}\frac{d\sigma_k}{dt} + \frac{\sigma_k}{\eta_k}\sigma = \sum\sigma_k \tag{2}$$

where G_k is the kth shear relaxation elastic modulus element and η_k is the kth viscosity element. Solving this equation gives:

$$\sigma_k = \varepsilon_0 G_k \exp(-t/\tau_k) \tag{3}$$

where $\tau_k (= \eta_k / G_k)$ is the relaxation time. By substituting Eq. (3) for Eq. (2), the relaxation elastic modulus G(t) in a generalized Maxwell model becomes the Prony series:

$$G(t) = G_0 + \sum_k G_k \exp(-t/\tau_k) \tag{4}$$

Therefore, once the master curve G(t) of the relaxation elastic modulus is obtained by a static stress relaxation test, the viscoelastic constants G_k and τ_k, are calculated by curve fitting.

Table 2 lists the elastic moduli, relaxation times, and viscosity coefficients obtained by model fitting. The 10 wt% Ref specimen present a low elastic modulus and a short relaxation time compared with neat EPDM/PP. This result demonstrates that the EPDM/PP matrix does not exhibit any reinforcement from the MWCNTs. However, 10 wt% Comp displays a higher elastic modulus than neat EPDM/PP, demonstrating that MWCNT disentanglement and dispersion promote reinforcement and cellulation contributes to the high elasticity of the matrix. In addition, it present a longer relaxation time is longer than neat EPDM/PP. It appears that this is a response of the region in which the MWCNTs are disentangled and dispersed and the cellulation structure is not formed and that this region thus provides the composite with flexibility. This may contribute to a high-flexibility and high-elasticity cellulation composite. These hypotheses will be verified by additional physical methods in future studies.

4. Conclusion

MWCNT/EPDM/PP composites were produced by resin elasto-milling and their structural and physical properties were measured. The new resin elasto-milling method promoted MWCNT disentanglement in a resin matrix. Composites containing at least 10 wt% disentangled MWCNTs exhibit unique properties, such as an increase of the yield strength, tensile strength, and storage elastic modulus (E′). These composites also display a stable storage elastic modulus range and suppressed migration at high temperature. These unique properties may stem from the three-dimensional cell structure formed in the matrix. These results are expected to improve mechanical and thermal properties of polymer matrices for practical use.

Acknowledgements

This research was partially supported by the Center of Innovation Program of the Japan Science and Technology Agency (JST) and the Strategic Core Technology Advancement Program (Supporting Industry Program) of the Chubu Bureau of Economy, Trade and Industry, and Exotic Nanocarbons, Japan Regional Innovation Strategy Program (JST).

References

[1] Oberlin A, Endo M, Koyama T. Filamentous growth of carbon through benzene decomposition. J Cryst Growth 1976;32(3):335–49.
[2] Endo M. Grow carbon fibers in the vapor phase. Am Chem Soc 1988;18(9):568–76.
[3] Iijima S. Helical microtubules of graphitic carbon. Nature 1991;354(6348):56–8.
[4] Allaoui A, Bai S, Cheng HM, Bai JB. Mechanical and electrical properties of a MWNT/epoxy composite. Compos Sci Technol 2002;62(15):1993–8.
[5] Sandler J, Shaffer MSP, Prasse T, Bauhofer W, Schulte K, Windle AH. Development of a dispersion process for carbon nanotubes in an epoxy matrix and the resulting electrical properties. Polymer 1999;40(21):5967–71.
[6] Gojny FH, Wichmann MHG, Fiedler B, Kinloch IA, Bauhofer W, Windle AH, et al. Evaluation and identification of electrical and thermal conduction mechanisms in carbon nanotube/epoxy composites. Polymer 2006;47(6):2036–45.
[7] Gojny FH, Wichmann MHG, Fiedler B, Schult K. Influence of different carbon nanotubes on the mechanical properties of epoxy matrix composites–a comparative study. Compos Sci Technol 2005;65(15):2300–13.
[8] Gojny FH, Wichmann MHG, Kopke U, Fiedler B, Schult K. Carbon nanotube-reinforced epoxy-composites: enhanced stiffness and fracture toughness at low nanotube content. Compos Sci Technol 2004;64(15):2363–71.
[9] Breton Y, Desarmot G, Salvetat JP, Delpeux S, Sinturel C, Beguin F, et al. Mechanical properties of multiwall carbon nanotubes/epoxy composites: influence of network morphology. Carbon 2004;42(5):1027–30.
[10] Gojny FH, Nastalczyk J, Roslanie Z, Schulte K. Surface modified multi-walled carbon nanotubes in CNT/epoxy-composites. Chem Phys Lett 2003;370(5):820–4.
[11] Ma P-C, Mo S-Y, Tang B-Z, Kim J-K. Dispersion, interfacial interaction and re-agglomeration of functionalized carbon nanotubes in epoxy composites. Carbon 2010;48(6):1824–34.
[12] Thostenson ET, Chou T-W. Processing-structure-multi-functional property relationship in carbon nanotube/epoxy composites. Carbon 2006;44(14):3022–9.
[13] Sánchez M, Campo M, Jiménez-Suárez A, Ureña A. Effect of the carbon nanotube functionalization on flexural properties of multiscale carbon fiber/epoxy composites manufactured by VARIM Carbon. Compos Part B 2013;45(1):1613–9.
[14] Saw LN, Mariatti M, Azura AR, Azizan A, Kim JK. Transparent, electrically conductive, and flexible films made from multiwalled carbon nanotube/epoxy composites. Compos Part B 2012;43(8):2973–9.
[15] Gkikas J, Barkoula N-M, Paipetis AS. Effect of dispersion conditions on the thermo-mechanical and toughness properties of multi walled carbon nanotubes-reinforced epoxy. Compos Part B 2012;43(6):2697–705.

[16] Damian CM, Garea SA, Vasile E, Iovu H. Covalent and non-covalent functionalized MWCNTs for improved thermo-mechanical properties of epoxy composites. Compos Part B 2012;43(8):3507–15.
[17] Yang Z, McElrath K, Bahr J, D'Souza NA. Effect of matrix glass transition on reinforcement efficiency of epoxy-matrix composites with single walled carbon nanotubes, multi-walled carbon nanotubes, carbon nanofibers and graphite. Compos Part B 2012;43(4):2079–86.
[18] Jiménez-Suárez A, Campo M, Sánchez M, Romón C, Ureña A. Influence of the functionalization of carbon nanotubes on calendaring dispersion effectiveness in a low viscosity resin for VARIM processes. Compos Part B 2012;43(8):3482–90.
[19] Lee SH, Cho E, Jeon SH, Youn JR. Rheological and electrical properties of polypropylene composites containing functionalized multi-walled carbon nanotubes and compatibilizers. Carbon 2007;45(14):2810–22.
[20] Pan Y, Li L, Chan SH, Zhao J. Correlation between dispersion state and electrical conductivity of MWCNTs/PP composites prepared by melt blending. Compos Part A 2010;41(3):419–26.
[21] Xiao Y, Zhang X, Cao W, Wang K, Tan H, Zhang Q, et al. Dispersion and mechanical properties of polypropylene/multiwall carbon nanotubes composites obtained via dynamic packing injection molding. J Appl Polym Sci 2007;104(3):1880–6.
[22] Micusik M, Omastova M, Krupa I, Prokes J, Pissis P, Logakis E, et al. A comparative study on the electrical and mechanical behaviour of multi-walled carbon nanotube composites prepared by diluting a masterbatch with various types of polypropylenes. J Appl Polym Sci 2009;113(4):2536–51.
[23] King J, Johnson BA, Via MD, Ciarkowski CJ. Effects of carbon fillers in thermally conductive polypropylene based resins. Polym Compos 2010;31(3):497–506.
[24] Xia H, Wang Q, Li K, Hu G-H. Preparation of polypropylene/carbon nanotube composite powder with a solid-state mechanochemical pulverization process. J Appl Polym Sci 2004;93(1):378–86.
[25] Yang J, Lin Y, Wang J, Lai M, Li J, Liu J, et al. Morphology, thermal stability, and dynamic mechanical properties of atactic polypropylene/carbon nanotube composites. J Appl Polym Sci 2005;98(3):1087–91.
[26] Teng C-C, Maa C-CM, Huang Y-W, Yuen S-M, Weng C-C, Chen C-H, et al. Effect of MWCNT content on rheological and dynamic mechanical properties of multiwalled carbon nanotube/polypropylene composites. Compos Part A 2008;39(12):1869–75.
[27] Lee G-W, Jagannathan S, Chae HG, Minus ML, Kumar S. Carbon nanotube dispersion and exfoliation in polypropylene and structure and properties of the resulting composites. Polymer 2008;49(7):1831–40.
[28] Funck A, Kaminsky W. Polypropylene carbon nanotube composites by in situ polymerization. Compos Sci Technol 2007;67(5):906–15.
[29] Prashantha K, Soulestin J, Lacrampe MF, Krawczak P, Dupin G, Claes M. Masterbatch-based multi-walled carbon nanotube filled polypropylene nanocomposites: assessment of rheological and mechanical properties. Compos Sci Technol 2009;69(11):1756–63.
[30] Bao SP, Tjong SC. Mechanical behaviors of polypropylene/carbon nanotube nanocomposites: the effects of loading rate and temperature. Mater Sci Eng A 2008;485(1):508–16.
[31] Jia Y, Peng K, Gon X-l, Zhang Z. Creep and recovery of polypropylene/carbon nanotube composites. Int J Plast 2011;27(8):1239–51.
[32] Ganß M, Satapathy BK, Thunga M, Weidisch R, Potschke P, Jehnichen D. Structural interpretations of deformation and fracture behavior of polypropylene/multi-walled carbon nanotube composites. Acta Mater 2008;56(10):2247–61.
[33] Thiébaud F, Gelin JC. Multiwalled carbon nanotube/polypropylene composites: investigation of the melt processing by injection molding and analysis of the resulting mechanical behavior. Int J Mater Form 2009;2(1):149–52.
[34] Koval'chuk AA, Shevchenko VG, Shchegolikhin AN, Nedorezova PM, Klyamkina AN, Aladyshev AM. Effect of carbon nanotube functionalization on the structural and mechanical properties of polypropylene/MWCNT composites. Macromolecules 2008;41(20):7536–42.
[35] King JA, Via MD, King ME, Miskioglu I, Bogucki GR. Electrical and thermal conductivity and tensile and flexural properties: comparison of carbon black/polycarbonate and carbon nanotube/polycarbonate resins. J Appl Polym Sci 2011;121(4):2273–81.
[36] Potschke P, Bhattacharyya AR, Janke A. Melt mixing of polycarbonate with multiwalled carbon nanotubes: microscopic studies on the state of dispersion. Eur Polym J 2004;40(1):137–48.
[37] Eitan A, Fisher FT, Andrews R, Brinson LC, Schadler LS. Reinforcement mechanisms in MWCNT-filled polycarbonate. Compos Sci Technol 2006;66(9):1162–73.
[38] Sennett M, Welsh E, Wright JB, Li WZ, Wen JG, Ren ZF. Dispersion and alignment of carbon nanotubes in polycarbonate. Appl Phys A 2003;76(1):111–3.
[39] Sun L, Jin-Tao Yang J-T, Lin G-Y, Zhong M-Q. Crystallization and thermal properties of polyamide 6 composites filled with different nanofillers. Mater Lett 2007;61(18):3963–6.
[40] Faghihi M, Shojaei A, Bagheri R. Characterization of polyamide 6/carbon nanotube composites prepared by melt mixing-effect of matrix molecular weight and structure composites. Compos Part B 2015;78:50–64.
[41] Liu T, Phang IY, Shen L, Chow SY, Zhang W-D. Morphology and mechanical properties of multiwalled carbon nanotubes reinforced nylon–6 composites. Macromolecules 2004;37(19):7214–22.
[42] Sengupta R, Ganguly A, Sabharwal S, Chaki TK, Bhowmick AK. MWCNT reinforced polyamide-6,6 films: preparation, characterization and properties. J Mater Sci 2007;42(3):923–34.
[43] Hana Z, Fina A. Thermal conductivity of carbon nanotubes and their polymer nanocomposites: a review. Prog Polym Sci 2011;36(7):914–44.
[44] Noguchi T, Magario A, Ueki H, Beppu J, Seki M, Iwabuki H, et al. Viscoelasticity and cellulation for carbon nanotube/elastomer composites. Polym Prepr Jpn 2006;55:3404.
[45] Noguchi T, Inukai S, Ueki H, Magario A, Endou M. Mechanical properties of MWCNT/elastomer nanocomposites and the cellulation model. SAE Tech Pap Ser 2009:5.
[46] Inukai S, Niihara K, Noguchi T, Ueki H, Magario A, Yamada E, et al. Preparation and properties of multiwall carbon nanotubes/polystyrene-block-polybutadiene-block-polystyrene composites. ACS Ind Eng Chem Res 2011;50(13):8016–22.
[47] Deng F, Ito M, Noguchi T, Wang L, Ueki H, Niihara K, et al. Elucidation of the reinforcing mechanism in carbon nanotube/rubber nanocomposites. ACS Nano 2011;5(5):3403.
[48] Endo M, Noguchi T, Ito M, Takeuchi K, Hayashi T, Kim YA, et al. Extreme-performance rubber nanocomposites for probing and excavating deep oil resources using multi-walled carbon nanotubes. Adv Funct Mater 2008;18(21):3403–9.
[49] Ito M, Noguchi T, Ueki H, Takeuchi K, Endo M. Carbon nanotube enables quantum leap in the oil recovery. Mater Res Bull 2011;46(9):1480–4.
[50] Endo M, Takeuchi K, Noguchi T, Asano Y, Kim YA, Hayashi T, et al. High performance rubber sealant for preventing water leaks. ACS Ind Eng Chem Res 2010;49(20):9798–802.
[51] MSC. Marc manual vol. A Ver. MSC Software Co; 20037.100–8.
[52] Christensen RM. Translated into Japanese. In: Kunio T, Miyano Y, editors. Theory of viscoelasticity, 1982. Yushodo Co., Ltd; 2000. p. 154–7.